Journal of Materials Chemistry A

PAPER

View Article Online
View Journal | View Issue

Cite this: J. Mater. Chem. A, 2014, 2, 7034

Energy level alignment of polythiophene/ZnO hybrid solar cells†

W. Feng,[a] S. Rangan,[b] Y. Cao,[c] E. Galoppini,[c] R. A. Bartynski[b] and E. Garfunkel*[ab]

Received 24th February 2014
Accepted 17th March 2014

DOI: 10.1039/c4ta00937a

www.rsc.org/MaterialsA

Energy level alignment at interfaces is critical for fundamental understanding and optimization of organic photovoltaics (OPV) as band offsets of the donor and acceptor materials largely determine the open circuit voltage (V_{oc}) of the device. Using ultraviolet photoemission spectroscopy (UPS) and inverse photoemission spectroscopy (IPS), we examined the correlation between energy level alignment and photovoltaic properties of a model bilayer hybrid solar cell incorporating electrodeposited polythiophene (e-PT) films on ZnO planar substrates. The electrolyte anion (BF_4^-, PF_6^-, ClO_4^- or $CF_3SO_3^-$) in the electrodeposition solution was found to have a strong influence on the e-PT film morphology and adhesion, the energy level alignment at the interface, and ultimately the V_{oc} of the photovoltaic devices.

1. Introduction

Electrodeposition of conductive polymers (electropolymerization) has been developed as an efficient synthetic method since its discovery in the late 1970s.[1] Recently, there is renewed interest in the field of polymer electrodeposition as prospects for efficient organic or hybrid organic–inorganic solar cells have greatly improved.[2–5] Electrodeposition, during which polymer synthesis and deposition occur simultaneously, is an alternative to conventional polymer deposition, which typically involves the chemical synthesis of the conductive polymers in solution and subsequent spin/drop-casting (often followed by thermal annealing to improve surface wetting). In contrast, electrodeposition is typically performed in a solution of monomers which is relatively inexpensive compared to commercially available polymers. Additionally, electrodeposition can be easily adapted to function in low-cost roll-to-roll processes compatible with mass production. Perhaps most importantly, electrodeposition offers conformal polymeric film on the substrate provided that the monomer diffusion is sufficient to reach the surface and reaction sites are uniformly distributed. For polymer integration into dense inorganic nanostructures such as vertically aligned high aspect-ratio nanorod/nanowires (*e.g.* ZnO nanorods,[2] CdS nanorods[3,4] and GaAs nanowires[5]), electrodeposition offers the advantage of satisfactory polymer infiltration by highly conformal polymer growth.

In order to optimize hybrid solar cells that incorporate electrodeposited polymers, it is critical to develop a fundamental understanding of energy level alignment at the interface as it has been found to affect organic photovoltaics (OPV) performance.[6] Recent literature studies of the interface between an organic phase (P3HT or PCBM) and an inorganic phase (ZnO) reveal charge transfer phenomena which result in an interface dipole and further establish the dependence of device parameters on the energy level alignment at the interface.[7–9] However, there has been limited study on the energy level alignment at the interface between electrodeposited polymers and inorganic materials. In this work, we use electrodeposited polythiophene (e-PT) and ZnO planar substrates as a model system to study the band offset at the interface and to determine its correlation with model device performance. Although this e-PT/ZnO model device does not represent an efficient OPV, it does serve as an excellent photovoltaic system to help develop a fundamental understanding of energy level alignment and its influence on device parameters.

Electrodeposition is controlled by a variety of factors including temperature, applied potential, total charge, electrolyte, monomer, solvent, the relative position of the electrodes, *etc.*[1,10] Previously, we studied the effects of solvent and total charge on the resulting film morphology.[2] In this paper, we examine the effect of the electrolyte on the structural and electronic properties of e-PT films and the energy level alignment at the interface between e-PT and ZnO. In particular, we focus on the electrolyte anion as it was shown to play a determining role on the polymer structure (the electrolyte cation only affects the behavior of polymer films during charge–discharge processes).[11,12]

The importance of the electrolyte anions is highlighted in the proposed mechanism of electropolymerization (Fig. 1). Polymerization is initiated by the formation of radical cations

[a]Department of Chemistry and Chemical Biology, Rutgers University, Piscataway, NJ 08854, USA. E-mail: egarf@rutgers.edu

[b]Department of Physics and Astronomy, Rutgers University, Piscataway, NJ 08854, USA

[c]Department of Chemistry, Rutgers University, Newark, NJ 07102, USA

† Electronic supplementary information (ESI) available. See DOI: 10.1039/c4ta00937a

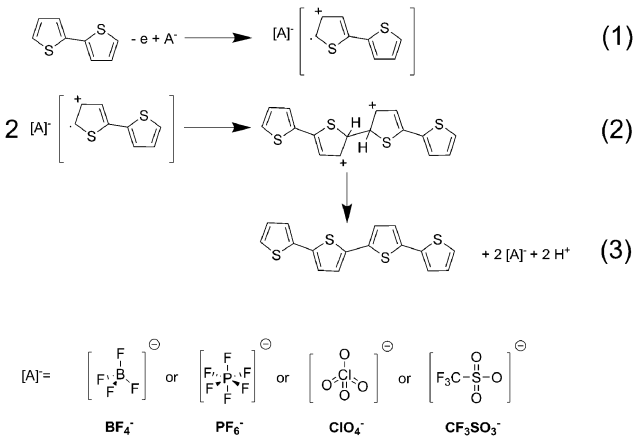

Fig. 1 Anion-assisted electrodeposition mechanism.

from monomers (2,2′-bithiophene), followed by the coupling of two radical cations to form a dimer. The dimer then reacts further and produces the polymer.[13] The anions in the electrolyte solution participate in the reaction by coordinating to the positively charged radical cations forming a so-called "ion pair", reducing the repulsive force experienced between the two radical cations when they approach and thereby facilitating the coupling reaction.[14,15] This "anion-assisted" polymerization mechanism shows the critical role of anions in determining the extent of polymer conjugation, which prompted our studies of the anion effect on the resulting polymer structural and electronic properties.

The electrolyte anions we chose to study are BF_4^-, PF_6^-, ClO_4^- and $CF_3SO_3^-$ (Fig. 1). These four anions were selected because they have different sizes, different extent of charge delocalization, and different basicity/electronegativity at the periphery of the anion.[16]

Many studies have been carried out to examine the anion effect on the nucleation and growth processes,[17] electrochemical[11] and electronic properties,[18] electrical conductivity,[19] and morphology[20] of the deposited polymer films. However, most of these studies focused on heavily doped "metallic" polymer films, which are not suitable as semiconductive materials in OPV. In our study, semiconducting polymer films with little or no dopant anions were produced to ensure that the dopant effects on the electronic properties were eliminated and that the observed electronic properties were primarily dependent on the polymer structure. We found that the electrolyte anions have a strong influence on the resulting film morphology and energy level alignment at the e-PT/ZnO interface. These effects, in turn, modulate the photovoltaic properties of the system. Such a correlated morphology/electronic/photovoltaic relationship provides an improved understanding for polythiophene/ZnO hybrid solar cells and could serve as a general model for other electropolymerized polymer/inorganic systems.

The chemical composition, optical properties, structural regioregularity and morphology of the electrodeposited neutral polymer films were characterized by X-ray photoemission spectroscopy (XPS), UV-vis absorption, FTIR-ATR and SEM, respectively. Ultraviolet photoemission spectroscopy (UPS) was employed to study the energy level alignment at the interface of e-PT and ZnO, aided by *ab initio* density of states (DOS) calculations. An interface dipole, defined in this paper as the vacuum level offset between e-PT and ZnO, was observed for certain e-PT/ZnO systems and was found to be largely responsible for improved open circuit voltage (V_{oc}) in model device testing. Cyclic voltammetry (CV) was used as a complementary method for estimation of the ionization potential (IP) values of the e-PT films and compared with results from UPS measurements. This multi-technique approach enables us to correlate the model device performance (in particular, V_{oc}) with the observed energy level alignment by UPS.

2. Results

2.1 Electrodeposition of polythiophene and dedoping

The general experimental scheme for the paper is illustrated in Scheme 1. Starting from a working electrode (WE) consisting of a ZnO film deposited on an ITO/glass substrate, electrodeposition was carried out by applying a sufficiently large potential to the WE relative to the reference electrode (RE) in the monomer solution. The as-deposited e-PT polymer chains are positively charged and heavily doped with the electrolyte anions (approximately 1 anion per 5 thiophene units according to our XPS study). Subsequently, this as-grown e-PT film was placed into a monomer-free solution for "dedoping", by applying a negative potential (−1 V) to the WE. This dedoping process removes the electrolyte anions from the as-deposited e-PT films and the resulting polymer chains are neutral. An electrochromic effect (film color change from dark blue to red, illustrated in Scheme 1) is associated with this dedoping process. The final polymer material after dedoping is a p-type semiconductor material[21–23] (for relevant *J*–*V* characterization of the dedoped e-PT, see ESI, Fig. S1†), making it suitable for integration into the active layer of our OPV devices.

Electrodeposition of polythiophene was carried out under potentiostatic conditions using 2,2′-bithiophene as the monomer. The potentiostatic method enables real-time electrochemical charge monitoring and thereby accurate control over e-PT film growth. In ideal conditions, the electrochemical charge is directly proportional to the resulting film thickness. The oxidation potential for 2,2′-bithiophene is 0.85–0.90 V,

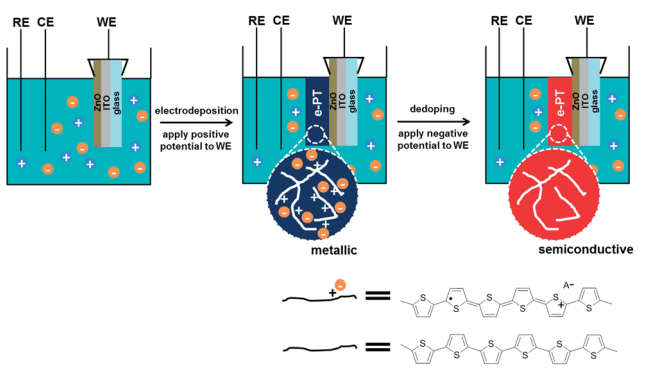

Scheme 1 Electrodeposition and dedoping (A^-: electrolyte anion).

which is 0.7 V lower than that of thiophene,[24] preventing polymer over-oxidation and chain mislinkages at a higher applied potential. To verify polymer structural regularity, FTIR-ATR studies (ESI, Fig. S2†) were carried out. The results show that, within instrumental resolution, all films were free of mislinkage (*i.e.* β-linkages) that may lead to a disruption of polymer conjugation and chain packing.

Four different electrolyte anions were used: BF_4^-, PF_6^-, ClO_4^- and $CF_3SO_3^-$. The minimum potential required to initiate electrodeposition was found to be 0.90 V for all electrolyte solutions, except for ClO_4^- solution in which polymerization could be initiated at a slightly lower potential of 0.85 V. The lowest potential necessary for deposition was applied because higher applied potentials lead to unwanted crosslinking or other side reactions[25] that may degrade the polymer's electronic properties and device performance. *I–t* curves obtained during the polymer growth are shown in Fig. 2. The electrochemical growth behavior can be generally described as "nucleation and growth": after a brief initial decrease in current (the induction period), polymeric nuclei begin to form and grow on the ZnO surface, corresponding to a slow continuous increase in current. This is then followed by a more rapid current increase (presumably as the nuclei cover the surface), which eventually slows down during steady state growth. Substantial current variations are measured from polymers produced in solutions containing different anions. Using BF_4^- and $CF_3SO_3^-$ resulted in significantly higher currents than PF_6^-. Growth with ClO_4^- gave rise to the lowest measured current, which is likely due to the slightly lower potential applied.

For simplicity and clarity in description, the final state of electrodeposited neutral polymer is referred as the "X^- polymer" (X^- represents the specific electrolyte anion used during electropolymerization). For example, for e-PT film grown in BF_4^- electrolyte solution and then electrochemically reduced to remove the BF_4^- anions, it would be called "BF_4^- polymer".

2.2 Chemical composition

XPS studies were carried out to analyze the chemical composition of the neutral polymer films and to examine whether the anion dopants were completely removed.

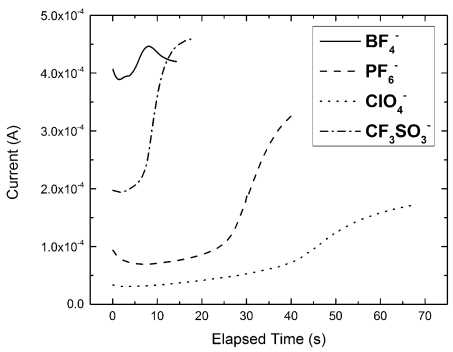

Fig. 2 *I–t* curves for the potentiostatic electrodeposition of polythiophene onto ZnO films in electrolyte solutions containing various anions: BF_4^-, PF_6^-, ClO_4^- and $CF_3SO_3^-$. The electrochemical charge is fixed at ~5 mC for all samples.

The C 1s and S 2p core level spectra of the neutral polymers grown with various electrolyte anions are shown in Fig. 3. A careful comparison of the lineshapes of these core levels can help in characterizing the C and S local environment. The C 1s lineshape can be decomposed into 6 components (binding energy values listed in Table S1†) as indicated in Fig. 3a. The component found around 284.2 eV was assigned to the aromatic α carbon in the thiophene ring,[26] whereas the one at 285.0 eV was assigned to the aromatic β carbon in the thiophene ring with a partial contribution from the adventitious carbon (resulting in an apparent higher intensity for the β carbon peak than the α carbon peak). At higher binding energy, carbon peaks of increasing binding energy at 286.1–286.5, 287.6–287.9, 288.9–289.6 and 290.4–290.7 eV were assigned to environments of increasing oxidation states. The intensities for these oxidized carbon peaks are small, therefore peak fitting (intensity and energy) can only achieve moderate accuracy, and consequently the information content is somewhat limited. Additionally, for conjugated carbon-based structures, a shake-up satellite is anticipated at ~6–7 eV higher binding energy relative to the main carbon peaks,[27] which places this satellite at ~290–292 eV. This region overlaps with that of the highest oxidized carbon

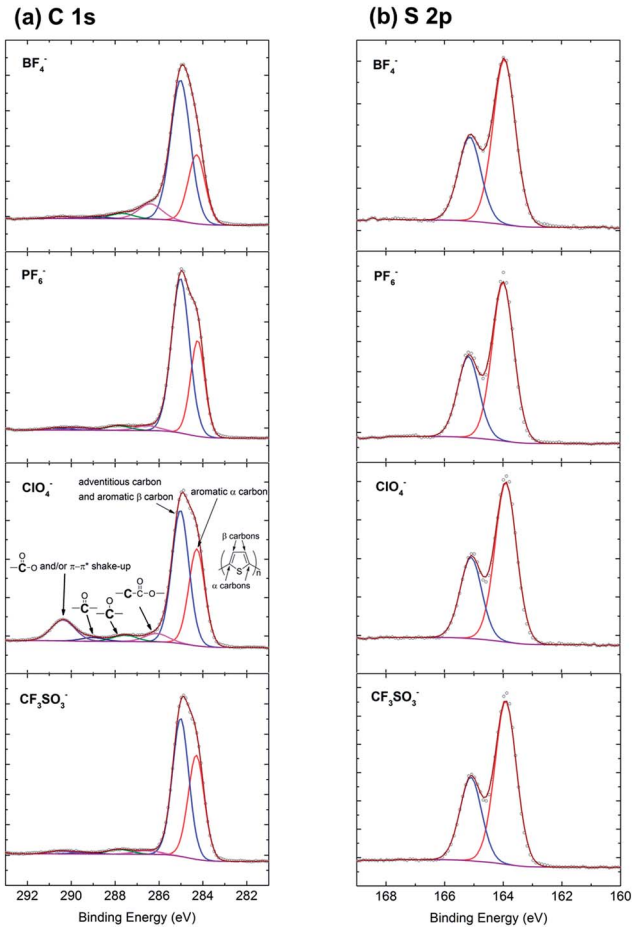

Fig. 3 (a) C 1s and (b) S 2p core level spectra of neutral polymers grown in the electrolyte solution containing the following anions: BF_4^-, PF_6^-, ClO_4^- and $CF_3SO_3^-$.

states. The polymer synthesized using ClO_4^- displays a higher shake-up intensity, indicating that this specific polymer is likely to have a higher conjugation length than the other polymers.

The S 2p core level spectra measured on the four polymer films are displayed in Fig. 3b. The characteristic lineshape is described by a single spin-orbit doublet, with the S $2p_{3/2}$ peak centered at 163.9–164.0 eV and assigned to sulfur in neutral thiophene.[28] For comparison purposes, the S 2p core level spectra of heavily anion-doped polythiophene samples typically have two more spin-orbit doublets corresponding to polaronic and multipolaronic states, with the multipolaron state being more significantly manifested as a higher energy tail 2.2 eV away from the neutral thiophene S peak (ESI, Fig. S3†).

For the polymers synthesized in BF_4^-, PF_6^- and $CF_3SO_3^-$, F 1s spectra (Fig. 4a–c) are used to quantify the dopant anion concentration within the polymer matrix. Both the polymers synthesized in BF_4^- and PF_6^- contain a signature of F^-, with F 1s peaks centered at 685.0 and 685.1 eV, respectively.[29] An additional F 1s peak is also visible at 687.1 eV for the polymer synthesized using PF_6^-, attributed to PF_6^- or PF_5.[29] For the polymer films synthesized using $CF_3SO_3^-$, no fluorine signal was measured within the detection limit of the XPS system. The unexpected presence of F^- in the polymers synthesized using BF_4^- or PF_6^- indicates that the BF_4^- and PF_6^- anions underwent a dissociation reaction and yielded F^- anions during the electrochemical deposition:[16]

$$BF_4^- \rightarrow BF_3 + F^-$$

$$PF_6^- \rightarrow PF_5 + F^-$$

As such, large and weakly coordinating BF_4^- and PF_6^- anions decomposed and yielded smaller and more strongly coordinating F^- anions. This reaction is present for BF_4^- and PF_6^- anions (but not for $CF_3SO_3^-$) and this must be taken into account when considering the anion effect on polymerization, as will be further explored in the Discussion section.

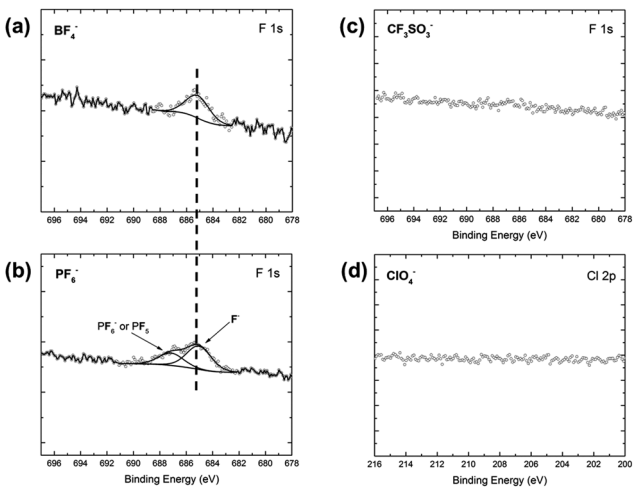

Fig. 4 F 1s core level spectra of neutral polymers grown in the electrolyte solution containing the following anions: (a) BF_4^-, (b) PF_6^- and (c) $CF_3SO_3^-$. (d) Cl 2p core level spectra of neutral polymers grown in the electrolyte solution containing ClO_4^-.

As sulfur is present in each thiophene unit of the backbone of the polymer, the concentration of dopant anions can be estimated using the atomic ratio of fluorine to sulfur (F : S). The F : S ratio obtained for the polymers is as follows: 2.8% for the BF_4^- polymer and 2.6% at most (considering that the higher binding energy peak is solely of PF_5) for the PF_6^- polymer. These ratio values reflect that in some of the polymers the dopant anion is difficult to be completely removed even upon reduction for a prolonged period of time. However, the extremely low concentration of dopant anion levels will not cause observable changes in the polymer electronic properties such as ionization potential (IP) as measured by UPS (ESI, Fig. S4†): this is evidenced by the polymer sample with a dopant concentration slightly higher at 3.2%, showing no significant change in IP compared to a dopant-free sample. Only at a much higher dopant anion level of 17% does the IP show an increase of 0.2 eV.

Finally, for the ClO_4^- polymer, there is no detectable dopant Cl 2p signal (Fig. 4d).

To summarize, the four polymer films obtained have no dopant anions left (ClO_4^- and $CF_3SO_3^-$) or have a very low concentration of dopant anions (BF_4^- and PF_6^-) that were found to exert no observable effect on the electronic properties measured by UPS.

2.3 Optical properties

UV-visible absorption spectra measured on a clean ZnO film and on the four polymers (in this case with a fixed polymerization charge of 50 mC) are shown in Fig. 5. In all spectra, the change in slope observed below ~400 nm leads to a high intensity background; this is attributed to the absorption of glass. Consequently, the ZnO absorption is small relative to the substrate background,[30] but can still be extracted using a proper spline background subtraction. The resulting absorption feature is shown in the inset of Fig. 5, and an extrapolation of the high-wavelength edge to the background of the spectrum leads to an optical gap of 376 nm (or 3.3 eV), in agreement with the typical value found for sol–gel produced ZnO films.[31] Given the high intensity of the polymers absorption edges, a simple extrapolation of the high-wavelength edge to the background of the spectra leads to an optical band gap of 2.0 eV for all polymers, independent of the anion used during electrodeposition. A similar behavior was previously reported for electrodeposited poly(3,4-ethylenedioxythiophene) (PEDOT) films using various anions in the electrolyte solution.[32]

2.4 Film morphology

In order to better understand the growth mechanism during electrodeposition, a clean ZnO surface and dedoped thin (polymerization charge of 5 mC) and thick (polymerization charge of 50 mC) polymer films were observed using SEM. It should be noted that there was no observable change in surface morphology or thickness before and after the dedoping process (ESI, Fig. S5†). This indicates that, when the polymer film is

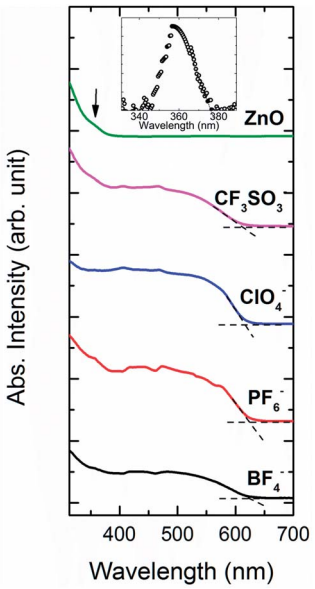

Fig. 5 UV-vis absorption spectra measured on a clean ZnO film and on the four undoped polymer films grown on ZnO for a fixed polymerization charge of 50 mC. The arrow points to a small shoulder on the ZnO/ITO/glass sample that is attributed to the absorption from ZnO. After proper background subtraction, a ZnO absorption feature can be extracted and shown in the inset.

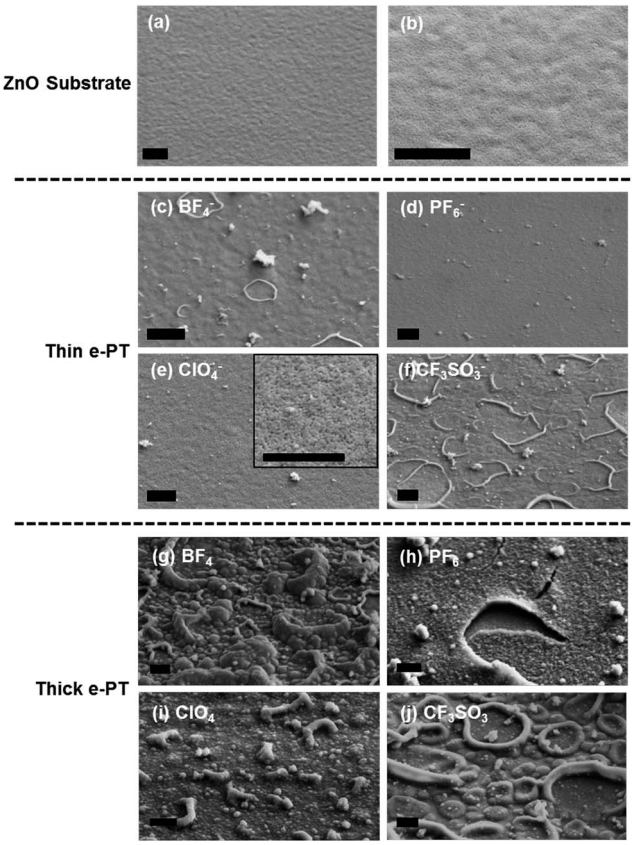

Fig. 6 Summary of SEM images. (a) ZnO film, (b) magnified view of ZnO film; thin e-PT films synthesized with 5 mC polymerization charge using the following electrolyte anions: (c) BF_4^-, (d) PF_6^-, (e) ClO_4^- and (f) $CF_3SO_3^-$; thick e-PT films synthesized with 50 mC polymerization charge using the following electrolyte anions: (g) BF_4^-, (h) PF_6^-, (i) ClO_4^- and (j) $CF_3SO_3^-$. All SEM images are taken from a 45° tilt angle. Scale bar = 1 μm.

removed from the solution and allowed to dry in air, it undergoes structural relaxation to relieve the stress that it experienced in the volume-expanding solvated state during electropolymerization. Dedoping does not induce noticeable further structural change in these samples.

The starting ZnO film (Fig. 6a and b) adopts a relatively porous structure typical of sol–gel produced ZnO films and exhibits wavy surface roughness. The thin films, polymerized with a charge of 5 mC (ESI, Fig. S6†), adopt various morphologies on the substrate (as shown in Fig. 6c–f), highlighting the effect of anions on polymer growth. There are several distinguishable features: (1) films: relatively continuous conformal layers of polymer; (2) fibers: extended irregular polymer structures resembling ridges or rings; (3) nodular deposits: clusters of loose polymer deposits on top of the thin film. Nodular deposits are present in all films. These features appear brighter in the SEM images because their protrusion causes more severe charge accumulation than other areas when exposed to the electron beam. They are likely diffusion-limited polymer aggregates.[33] It is thought that increased interactions among the anions, the solvent-swollen polymer and the oligomers, resulted in these insoluble aggregates on the polymer film.[20] They extend away from the polymer film as they grow and are scattered across the entire surface with what appear to be high surface area structures. Fiber deposits (appearing bright in SEM images for the same reason mentioned above for the nodular deposits) were found for the BF_4^- and $CF_3SO_3^-$ polymers, but not the PF_6^- or ClO_4^- ones. The overall surface of the thin BF_4^- and $CF_3SO_3^-$ polymers appear to be continuous, with morphology closely resembling that of the underlying ZnO substrate, and bearing a similar wavy appearance. However, the PF_6^- polymer film is relatively smooth and does not appear to share the same undulating roughness of the underlying ZnO substrate as it does in the other two films. Finally, the ClO_4^- polymer displays a rather open structure (Fig. 6e), with noticeably less film compactness than the other three polymers.

By increasing the electrochemical charge from 5 mC to 50 mC, much thicker films were produced (~80 nm, ESI, Fig. S7†). These thicker films generally show a trend of more pronounced morphological features (Fig. 6g–j) as compared to their thinner counterparts. The BF_4^- and $CF_3SO_3^-$ polymers follow a similar growth pathway, where the relatively small number of fiber deposits originally seen in the thin films changed to larger size and greater numbers of fibers or circularly shaped deposits. This translates into higher roughness overall compared to their thinner counterparts. The ClO_4^- polymers become more dense and compact compared to what is observed at the early stage of growth, with similarly fiber-shaped polymer deposits on the film surface but comparatively less rough than the BF_4^- and $CF_3SO_3^-$ polymers. A unique aspect of the PF_6^- polymer is the appearance of morphological defects in the form of extensive cracks on the film surface, presumably

because the film cannot withstand the large surface tension experienced from the solvent-swollen state in solution to the dried state when taken out of the solution and allowed to dry in air. This also demonstrates poor film adhesion of PF_6^- produced polymer films to the ZnO substrate, which has also been observed for the thinner film.

2.5 Electronic structure at the e-PT/ZnO interface

2.5.1 UPS/IPS studies of ZnO films. The valence bands (VB) and conduction bands (CB) of pristine ZnO films have been probed using UPS and IPS. It should be noted that our UPS measurements have an error bar of ±0.1 eV due to instrumental broadening. Typical VB and CB spectra are shown in Fig. 7a. The He II VB spectrum is characterized by a strong signal from the shallow Zn 3d core levels at 11.3 eV, and by well-defined O 2p states ranging from ~4–9 eV. The conduction band of ZnO is typically featureless, due to the low inverse photoemission cross section of the Zn 4s–4p states. As both occupied and unoccupied states are referenced with respect to a common Fermi level, and analyzed in the same UHV system, an energy gap can be directly extracted from the valence and conduction band edges. Using a linear extrapolation of the leading edge to the background of the spectra, a valence band edge of 3.5 eV and a conduction band edge of −0.1 eV are obtained, defining a 3.6 eV transport gap for the ZnO film.

The UPS He I spectrum of the pristine ZnO surface is shown in Fig. 7b. The secondary electron cutoff energy (E_{SEC}) as well as the valence band edge energy (E_{VBE}) are extracted using the same linear extrapolation method mentioned above. From these values, the ionization potential (denoted as IP and defined as the distance from the VBE to the vacuum level) can be calculated using the following equation:

$$IP = h\nu - |E_{SEC} - E_{VBE}| \quad (1)$$

where $h\nu$ is the incident He I line energy at 21.2 eV, E_{SEC} at 17.5 eV and E_{VBE} at 3.6 eV. Therefore the calculated IP for ZnO is 7.3 eV, similar to literature values.[34]

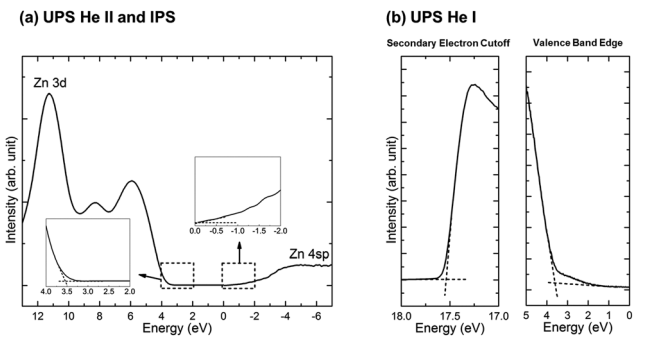

Fig. 7 (a) Valence (E > 0) and conduction (E < 0) band edge spectra measured on a pristine ZnO film using UPS and IPS, respectively. The spectra are both referenced to the Fermi level of the system (E = 0). The band edges onsets are indicated in the inset. (b) Details of the secondary electron cutoff and valence band edge obtained on the pristine ZnO film.

2.5.2 UPS studies of e-PT films. Before examining the experimental electronic structure obtained from the four polymer films, it is useful to consider the calculated density of states (DOS) of thiophene and oligothiophenes (restricted to head-to-tail molecular geometries), shown in Fig. 8a. As expected, the increasing delocalization of the π system with increasing polymer unit length leads to a progressive reduction of the HOMO–LUMO gap (indicated with dashed lines), along with the development of well-defined molecular band structures. Details of the DOS of a sexithiophene unit (6 T) as well as the main orbital character constituting the electronic structure are presented in

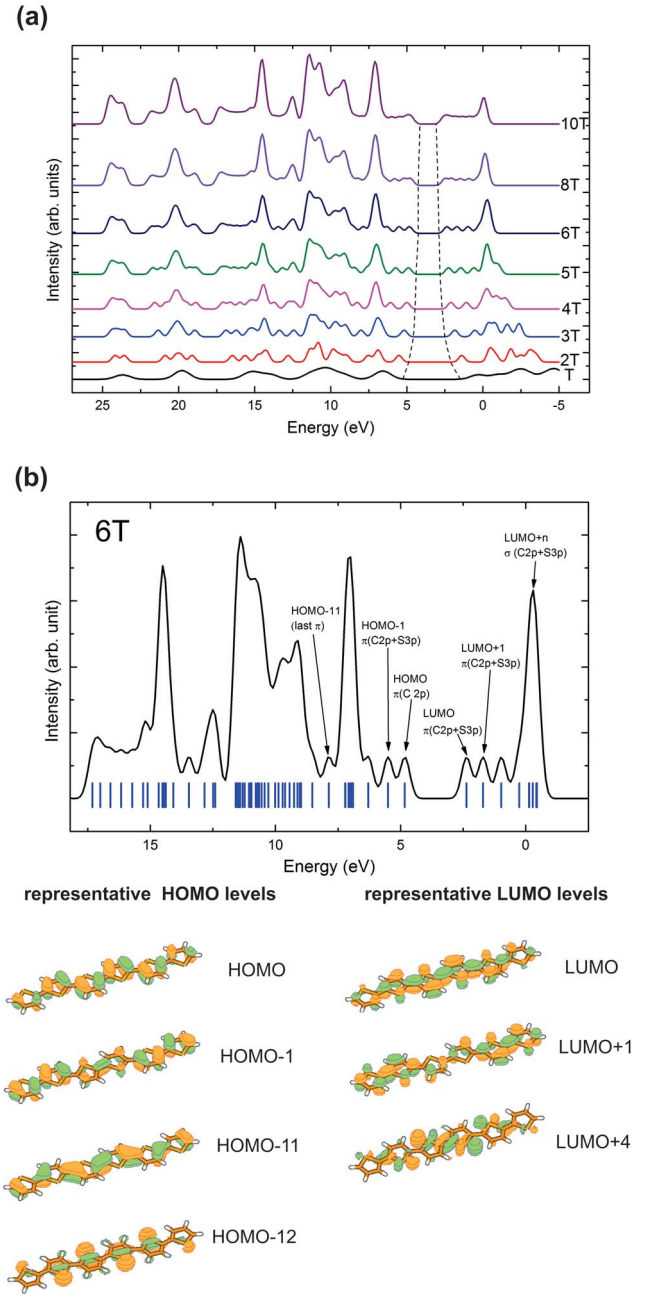

Fig. 8 (a) Calculated DOS spectra of thiophene (T) and oligothiophenes (2 T–10 T). (b) Assignment and contour plots of representative HOMO and LUMO levels for sexithiophene (6 T).

Fig. 8b. In agreement with previous theoretical UPS work,[35] the HOMO found at 4.8 eV is of π(C 2p) character, while the HOMO−1 state at 5.5 eV is of π(C 2p + S 3p) character. Multiple π states are found at higher binding energies, followed by a large band of σ(C 2p + S 3p) states starting above 8.5 eV. In the unoccupied states, the first four individual molecular orbitals are π*(C 2p + S 3p), followed by σ*(C 2p + S 3p).

The experimental UPS He II valence band spectra of the four polymers (grown with a low electrochemical charge of 5 mC to obtain a very thin film such that interface electronic structure information can be extracted) are displayed in Fig. 9. Although the average chain length of the polymer is unknown, a comparison of the experimental valence band spectra to the DOS of a 6 T unit proves to be insightful. The calculated DOS for a 6 T unit has thus been added below the experimental valence band spectra, rigidly shifted in energy so as to align obvious experimental and theoretical features. The valence band features measured on the BF_4^-, PF_6^- and $CF_3SO_3^-$ synthesized polymers resemble the calculated DOS, modulated by the appearance of states characteristic of ZnO around 5 and 11 eV. In the case of the ClO_4^- polymer, the contribution of the underlying ZnO is more prominent, consistent with SEM observations (Fig. 6e). Thus the experimental VB of the four polymers can be described as follow: at energies below 5 eV we found strong π(S 3p + C 2p) states, followed by σ(C 2p + S 3p) states at energies greater than 5 eV.

Having established the nature of the valence band states for the polymer films, the HOMO onset can be extracted from the He II VB spectra of Fig. 10. The E_{VBE}, defined as the energy separation between the HOMO edge and the Fermi level, is reported in Table 1 for each polymer. The IP values for the polymers can also be extracted from the He I VB spectra measured on films biased at −5 V. The IP, defined as the energy difference between the vacuum level and the HOMO onset, is obtained analogous to how it was obtained for ZnO, using the

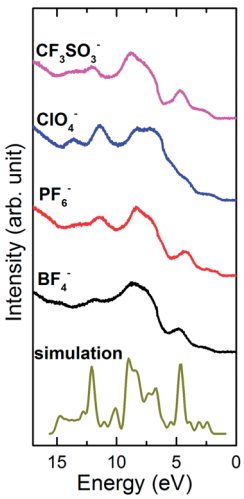

Fig. 9 Experimental UPS spectra of neutral polymer films synthesized using the following electrolyte anions: BF_4^-, PF_6^-, ClO_4^- and $CF_3SO_3^-$. The calculated DOS spectrum for sexithiophene (6T) is presented for comparison.

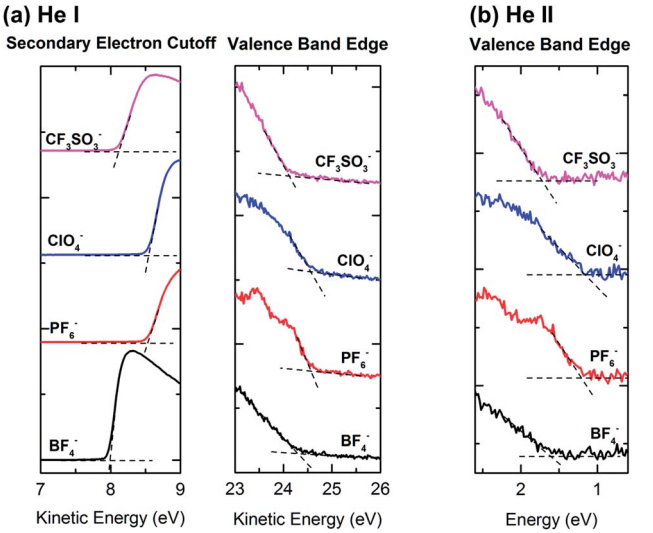

Fig. 10 Experimental UPS (a) He I spectra of the secondary electron cutoff and valence band edges; (b) He II spectra of the valence band edge.

E_{SEC} and E_{VBE} values from UPS He I and eqn (1). The extrapolation procedure for the relevant energy edges was displayed in Fig. 10 and the calculated IP values for the polymers prepared in various electrolyte solutions are tabulated in Table 1. The range of IP values (5.1–5.4 eV) was found to be similar to that obtained by a complementary technique, cyclic voltammetry (4.9–5.2 eV, ESI, Fig. S8†). From the IP and E_{VBE} values, we have also calculated the energy separation between the Fermi level and the vacuum level (E_F to E_v) by subtracting E_{VBE} from IP.

2.6 Photovoltaic testing of model device

Photovoltaic devices (Ag/e-PT/ZnO/ITO) were fabricated without thermal annealing (Fig. 11). The e-PT films were electrodeposited for a fixed charge of 50 mC to obtain a polymer layer of ~80 nm thick with a complete coverage over the ZnO substrate to prevent device shorting. Due to the PF_6^- polymer film exhibiting stress failure cracks across the substrate (Fig. 6h), the PF_6^- devices often shorted, as the underlying ZnO is partially exposed during Ag electrode deposition. The other three polymer films (BF_4^-, ClO_4^- and $CF_3SO_3^-$), however, had no such morphological defects and were successfully fabricated into solar cell devices. The resultant device parameters (J_{sc}, V_{oc}, FF and η) are displayed in Table 2.

Table 1 Summary of UPS data[a]

	He I			He II	
	E_{SEC} (KE)	E_{VBE} (KE)	IP	E_{VBE}	E_F to E_v
BF_4^- polymer	8.0	24.3	4.9	1.6	3.3
PF_6^- polymer	8.5	24.6	5.1	1.2	3.9
ClO_4^- polymer	8.5	24.6	5.1	1.2	3.9
$CF_3SO_3^-$ polymer	8.1	24.1	5.2	1.7	3.5

[a] SEC: secondary electron cutoff; VBE: valence band edge; IP: ionization potential; E_F: Fermi level; E_v: vacuum level; KE: kinetic energy.

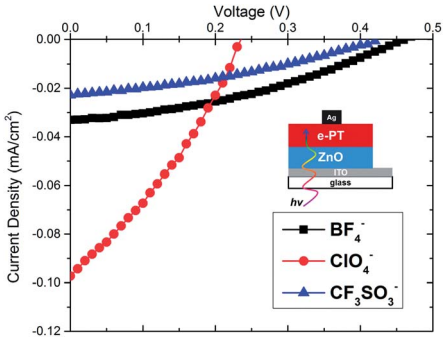

Fig. 11 Photovoltaic testing of e-PT/ZnO hybrid solar cells, of which the e-PT was synthesized using BF_4^-, ClO_4^- and $CF_3SO_3^-$ anions.

For comparison, a planar bilayer photovoltaic device which incorporates a commonly used and chemically synthesized conductive polymer, regioregular-P3HT (rr-P3HT) spin coated onto ZnO film, yielded J_{sc} of 0.25 mA cm^{-2}, V_{oc} of 0.30 V, FF of 0.38 and η of 0.029%. The main difference between rr-P3HT/ZnO and e-PT/ZnO devices is J_{sc}, which could be due to a number of factors, such as different optical absorption, film porosity and/or carrier mobility. We would like to emphasize that although our e-PT is not a high performing polymeric material, it is studied as a model to help us understand the relationship between the interfacial energy level alignment and device parameters, and to shed light on OPV design rules with an emphasis on the critical interface between the two phases.

Among the working photovoltaic devices, the ClO_4^- device shows a significantly higher J_{sc} of 0.097 mA cm^{-2} than the other two devices. This is most likely due to the higher conjugation length and packing order within this polymer. It could also be related to a number of factors, such as different optical absorption, film porosity and/or carrier mobility. This finding was found to correlate with results from our XPS (Fig. 3) and CV studies (ESI, Fig. S8†), both of which indicated higher regioregularity for the ClO_4^- polymer. Although the V_{oc} of the ClO_4^- device is lower than the other two polymers, it still has the best device efficiency thanks to a much superior J_{sc}.

The V_{oc} values for the BF_4^- and $CF_3SO_3^-$ devices, are 0.47 and 0.43 V, respectively (Table 2). These V_{oc} values are comparable with those observed for typical PT/ZnO hybrid solar cells.[36] The ClO_4^- device shows a lower V_{oc} of 0.24 V (Table 2), which is ~0.2 V lower than the other two hybrid devices. The difference between the actual V_{oc} values of these devices likely originates from the interfacial energy level alignment and is discussed further in the following Discussion section.

Table 2 Summary of photovoltaic properties

Device	J_{sc} (mA cm^{-2})	V_{oc} (V)	FF	η
BF_4^-	0.033	0.47	0.36	0.0057%
ClO_4^-	0.097	0.24	0.31	0.0073%
$CF_3SO_3^-$	0.023	0.43	0.34	0.0033%

3. Discussion

Based on the polymerization mechanism outlined in the introduction, the coordinating ability of the anions (BF_4^-, PF_6^-, ClO_4^- and $CF_3SO_3^-$) to the positively charged monomeric and oligomeric thiophene species in the solution is thought to regulate the extent of conjugation. Both molecular volume of the anion and the basicity of the peripheral atoms within the anion, were found to affect its coordinating ability.[16] A larger anion has a more delocalized charge distribution and thus a weaker coordinating ability. In addition, anions with fluorine atoms at the periphery should be more weakly coordinating than those with more accessible oxygen atoms: studies have shown that BF_4^- or PF_6^- have weaker coordinating ability than ClO_4^- or $CF_3SO_3^-$.[16]

As for BF_4^- and PF_6^- anions, the molecular volumes were found to be 53.4 and 73.0 $Å^3$, respectively.[37] If the molecular volume was the sole determining factor for coordinating ability, PF_6^- should have the weaker coordination ability of the two. However, the discrepancy in coordinating ability of these two anions in the literature point to other contributing factors such as the Lewis acid character of the boron atom and the variation in coordination to different molecular systems.[38–41] To complicate matters further, large and weakly coordinating anions can dissociate into smaller and more strongly coordinating anions. In our experiments, PF_6^- and BF_4^- decompose into F^-, further complicating the analysis of the results. Based on the above considerations, it is not entirely straightforward to decouple the coordinating ability of the anions from the resulting polymer conjugation process.

Despite the complexity of the anion effect, we are still able to find a reasonable correlation between the polymer morphology, interfacial energy level alignment, and the photovoltaic properties of e-PT/ZnO hybrid solar cells. From UPS measurements on a clean ZnO substrate and four polymer thin films, together with the optical bandgap information for the polymers, a diagram representing the energy level alignment at the ZnO–polymer interface can be constructed (Fig. 12). The interface dipole (Δ), is defined as the vacuum level offset between e-PT and ZnO substrate. A negative Δ value means that the e-PT vacuum level is lower than the ZnO vacuum level, whereas a positive Δ value indicates the opposite.

The IP (HOMO to vacuum level) values by UPS are 4.9, 5.1, 5.1, 5.2 eV for BF_4^-, PF_6^-, ClO_4^- and $CF_3SO_3^-$ polymers, respectively. Considering the instrumental resolution (±0.1 eV), the measured IP values can be considered to be relatively close in range. It is therefore the interface dipole that is causing a more pronounced difference in the energy separation between the polymer HOMO and the ZnO valence band, which represents the theoretical V_{oc} of these e-PT/ZnO hybrid solar cells. The interface dipole in effect "pushed" the HOMO levels of the BF_4^- and $CF_3SO_3^-$ polymers down by 0.5 eV and 0.3 eV, respectively, while the absence of such an interface dipole (the small value of +0.1 eV is within the experimental error) for PF_6^- and ClO_4^- polymers did not change the HOMO levels for these two polymers. This leads to a larger theoretical V_{oc} for BF_4^- and $CF_3SO_3^-$ devices compared to the other devices.

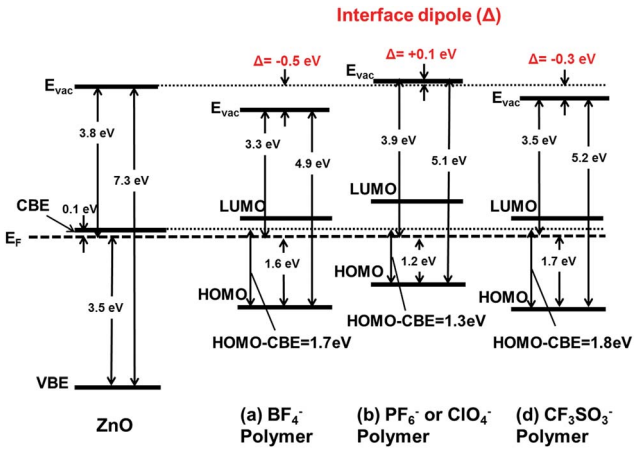

Fig. 12 Energy level alignment at the interface of ZnO and neutral e-PT polymer film synthesized in electrolyte solutions containing BF_4^-, PF_6^-, ClO_4^- or $CF_3SO_3^-$ (the PF_6^- and ClO_4^- polymers have similar energy levels).

The existence of such an interface dipole likely stems from the interaction between the polymer films and the underlying ZnO substrate. The interface dipole can be explained by an integer charge-transfer model.[42] The dipole is created by charge transfer at the interface, with electronic charges usually transferred from the polymer to ZnO producing a positively charged polymer and a negatively charged ZnO. Such an interface dipole downshifts the polymer vacuum level with respect to the ZnO vacuum level. Interface dipoles between the organic and inorganic phase (similar to our polythiophene/ZnO system) has also been observed by others.[7–9,43] Recent work shows that the interfacial dipole moment (both its intensity and direction) affects V_{oc}.[44]

It should be noted that we have also investigated the dopant concentration at the e-PT/ZnO interface, which represents another possible factor that may influence the energy level alignment at the interface. From the XPS depth profile (ESI, Fig. S9†), there is no obvious residual anion dopant gradient detected from the surface of a thick e-PT film to the interface of e-PT/ZnO. Therefore, the possibility of the dopant concentration as a contributor to the interface dipole is ruled out.

Photovoltaic studies showed that BF_4^- and $CF_3SO_3^-$ devices have V_{oc} values that are about 0.2 V higher than those for ClO_4^- devices. In comparison, as discussed above, the interfacial energy level alignment determines that the theoretical V_{oc} values for BF_4^- and $CF_3SO_3^-$ devices are 0.4–0.5 eV higher than that for the ClO_4^- device. Various loss processes lead to less pronounced differences between theoretical and actual V_{oc} values.[36] From the studies of theoretical and actual V_{oc} values of these model devices, we have demonstrated a correlation between energy level alignment at the interface and the device V_{oc}, and further confirmed the commonly accepted origin of the theoretical V_{oc}: relative band offsets of the two phases.

4. Conclusions

We have studied the effect of electrolyte anions on the structure of electrodeposited neutral polythiophene films on planar ZnO substrates, and on the energy level alignment at the polymer/ZnO interface. The origin of the anion effect arises from its coordination with the relevant radical cations before the species undergo coupling reactions and form longer conjugation units. XPS studies have identified dissociation reactions under our electrochemical conditions, wherein F^- anions were produced and were presumably more strongly coordinating than the larger anions BF_4^- and PF_6^-. This scenario complicates a direct comparison of coordinating ability among these four anions based on coordination rules for weakly coordinating anions.

Although the difference in the IP values for all relevant polymers remains small (0.2–0.3 eV), the interface dipole (energy offset in the vacuum levels between e-PT and ZnO) "pushed" the HOMO levels of the polymer down in two (BF_4^- and $CF_3SO_3^-$) of the four polymers, and resulted in a larger difference of 0.4–0.5 eV between the polymer HOMO level and ZnO CB. This latter observation is directly related to the photovoltaic properties of e-PT/ZnO hybrid solar cells as it represents the theoretical V_{oc}. The establishment of a correlation between the theoretical and actual V_{oc} values further validates the model that V_{oc} is determined by the relative band alignment at the interface. Although the device efficiencies are relatively low, our fundamental studies using e-PT/ZnO as model photovoltaic systems have demonstrated the role of interface dipole in regulating solar cell properties, especially by controlling the V_{oc}.

5. Experimental

5.1 Materials

Zinc acetate dihydrate (99%, Aldrich), ethanolamine (99%, Aldrich), 2,2′-bithiophene (98%, TCI America), tetra-*n*-butylammonium tetrafluoroborate (Bu_4NBF_4, 98%, Oakwood Chemical), tetrabutylammonium hexafluorophosphate (Bu_4NPF_6, 98%, Aldrich), lithium perchlorate ($LiClO_4$, 99%, Alfa Aesar), tetra-*n*-butylammonium trifluoromethanesulfonate ($Bu_4NCF_3SO_3$, 98%, Alfa Aesar), 2-methoxyethanol (99%, Acros), acetonitrile (anhydrous, 99.8%, Alfa Aesar) were used without further purification. ITO-coated glass slides (MTI Corporation) were subjected to successive 10 minute ultrasonication in dichloromethane and acetone before being blown dried in a stream of nitrogen.

5.2 Synthesis of ZnO planar substrates

ZnO films were made by a sol–gel method.[45] A 750 mM zinc acetate solution in 2-methoxyethanol of equal molar ratio of zinc acetate and ethanolamine, was spin-coated at 2500 rpm for 30 seconds. The sol–gel films were annealed on a hot plate in air at 300 °C for 10 min. This sol–gel method afforded ZnO films ~30–40 nm thick.

5.3 Electrodeposition and electrochemical analysis

Electrodeposition experiments were carried out with a Princeton Applied Research potentiostat VersaSTAT 3. A three-electrode system was used. The working electrode was the ZnO planar substrate with a surface area of ~1 cm^2 immersed in the solution. The counter electrode was Pt gauze. The reference

electrode was a Ag/Ag^+ non-aqueous reference electrode consisting of a Ag wire immersed in acetonitrile (ACN) solution of 0.01 M $AgNO_3$ and 0.1 M Bu_4NPF_6. All potentials reported in this paper were referenced to this Ag/Ag^+ reference electrode. The electrochemical cell contained ~12 mL solution of 7.5 mM 2,2′-bithiophene and 0.1 M supporting electrolyte in ACN. Before electrodeposition, the solutions were de-oxygenated by bubbling nitrogen through the solution for 10 minutes; a nitrogen overpressure was maintained throughout the experiment. The e-PT films were electrodeposited using the potentiostatic method, which is to keep the potential constant and record the current–time (I–t) curves during film growth. The sample was then removed from the solution and rinsed with ACN. The sample was reduced by a standby potential of −1 V (*vs.* Ag/Ag^+ reference electrode) in a monomer-free electrolyte solution until the current was stable. The sample was again removed from solution and rinsed thoroughly.

For electrochemical analysis, cyclic voltammetry was carried out in a monomer-free electrolyte solution by sweeping the potential from −1 V to 1.3 V, at a rate of 0.05 V s^{-1}. The oxidation onset (E_{ox}) was converted to an ionization potential (IP) for the polymer based on the following considerations. Following the IUPAC recommendation of using a ferrocene/ferrocenium (Fc/Fc^+) redox couple in non-aqueous solutions for an internal standard, redox waves of Fc/Fc^+ were measured with 3 mM ferrocene in ACN.[46] The half-wave potential ($E_{1/2}$) was measured to be 0.1 V against Ag/Ag^+ reference electrode. The absolute potential value for Fc/Fc^+ must be established to reference our measured potential values to the vacuum level. Recent experimental and theoretical studies on the absolute potential of Fc/Fc^+ in ACN have determined it to be at 5.0 eV.[47,48] Such a value also agrees with earlier results on Fc/Fc^+ in aqueous solution and referencing it to the absolute potential of a standard hydrogen electrode (SHE).[47,49] Therefore, all E_{ox} values can be converted to the corresponding IP values: $IP = e(E_{ox} - 0.1\ V + 5.0\ V) = e(E_{ox} + 4.9\ V)$.

5.4 Model device fabrication and testing

Electrodeposition using 50 mC electrochemical charge produced e-PT films of ~100 nm on ZnO substrates. The top Ag electrode with an electrode area of 0.03 cm^2, was thermally evaporated in vacuum with a base pressure $\leq 1 \times 10^{-6}$ Torr. Photovoltaic J–V characterization was carried out using a HP 4140B pA meter/DC voltage source under AM 1.5 irradiation (100 mW cm^{-2}) with a 300 W xenon solar simulator. A Labview program was used with the solar simulator and the electrical characterization equipment through which voltages between −1 V and 1 V were delivered to the solar cell with a step size of 10 mV.

5.5 Characterization methods

X-ray photoemission spectroscopy (XPS) and ultraviolet photoemission spectroscopy (UPS) measurements were performed on as-loaded samples using a Thermo Scientific ESCALAB 250Xi with a base pressure $\leq 1 \times 10^{-9}$ Torr. The core level spectra were obtained with an Al-K_α monochromated X-ray source, resulting in a total instrumental broadening of 0.5 eV. The binding energy of the core levels was referenced to the adventitious C 1s peak set at 285.0 eV. UPS valence band spectra were obtained using a helium discharge source resulting in lines at 21.2 eV (He I) and 40.8 eV (He II), with a total instrumental broadening of 0.1 eV. The energy scale of the He II valence band spectra was referenced to the Fermi level of the system and set at 0 eV, measured on a sputter-cleaned Au sample in contact with the films. Work function measurements were performed using the He I line, with a negative bias of 5 V to the sample to help isolate the secondary electron cutoff of the films.

XPS depth profile by Ar^+ sputtering was performed on a Thermo Scientific K-Alpha system. Beam energy was set to 500 eV at low current, with a raster size of 1.2 mm. Under this condition, the estimated sputter rate (calibrated for Ta_2O_5) is 0.15 nm s^{-1}. The etching time per cycle is 100 seconds.

Band edges measurements were performed on ZnO in a separate UHV chamber housing both UPS and inverse photoemission spectroscopy (IPS) with a respective resolution of 0.3 eV and 0.6 eV, with details described elsewhere.[50] Both the valence band and conduction band spectra were referenced to the Fermi level of a sputter-cleaned Au sample in contact with the ZnO sample, and set as 0 eV.

DFT electronic structure calculations of the gas phase molecules were performed with the GAMESS(US) software package[51] using Becke3-Lee-Yang-Parr (B3LYP) hybrid functional.[52–54] Geometries of local minima on the potential energy surface were calculated with a 6-31G basis set either in the C_i or C_{2v} symmetry.[55] The density of states (DOS) was calculated by summing the individual electronic states convoluted with a 0.4 eV full width half maximum Gaussian function.

UV-visible absorption spectra were recorded on a Shimadzu UV-3600 UV-Vis-NIR spectrophotometer. The morphology of e-PT films was visualized by scanning electron microscope (Zeiss Sigma Field Emission SEM, 4 kV acceleration voltage) and helium ion microscope (HIM, Zeiss Orion Plus, 30 kV acceleration voltage, 0.2–0.4 pA beam current). Single attenuated total reflectance infrared (FTIR-ATR) experiments were performed on a Thermo Electron Corporation Nicolet 6700 FT-IR (ZnSe crystal, the number of spectra averaged is 1024 with a resolution of 4 cm^{-1}).

Acknowledgements

The authors would like to thank Dr. Samir Shubeita and Prof. Torgny Gustafsson for assistance in HIM imaging, supported by National Science Foundation (DMR-1126468). The authors would also like to thank Dr. Robert Ianniello and Prof. George Chen for helpful discussion. E. Galoppini and R.A.B. thank the Division of Chemical Sciences, Geosciences, and Biosciences, Office of Basic Energy Sciences of the U.S. Department of Energy (DE-FG02-01ER15256). Financial support from the National Science Foundation (DMR-1006740) for this work is gratefully acknowledged.

Notes and references

1 J. Roncali, *Chem. Rev.*, 1992, **92**, 711–738.
2 W. Feng, A. S. Wan and E. Garfunkel, *J. Phys. Chem. C*, 2013, **117**, 9852–9863.

3 D. Xi, H. Zhang, S. Furst, B. Chen and Q. Pei, *J. Phys. Chem. C*, 2008, **112**, 19765–19769.
4 B. Sun, Y. Hao, F. Guo, Y. Cao, Y. Zhang, Y. Li and D. Xu, *J. Phys. Chem. C*, 2011, **116**, 1395–1400.
5 M. Giacomo, Y. Wang, P.-S. Wong, A. Lech, C.-H. Hung, J. Shapiro, S. Prikhodko, M. El-Kady, R. B. Kaner and D. L. Huffaker, *Nano Lett.*, 2012, **12**, 3581–3586.
6 M. C. Scharber, D. Muhlbacher, M. Koppe, P. Denk, C. Waldauf, A. J. Heeger and C. J. Brabec, *Adv. Mater.*, 2006, **18**, 789–794.
7 J. H. Lee, J.-H. Shin, J. Y. Song, W. Wang, R. Schlaf, K. J. Kim and Y. Yi, *J. Phys. Chem. C*, 2012, **116**, 26342–26348.
8 S. J. Han, A. A. D. T. Adikaari, K. D. G. I. Jayawardena, N. A. Nismy, Y. H. Kim, J. W. Kim, Y.-B. Hahn and S. R. P. Silva, *Appl. Phys. Lett.*, 2013, **102**, 081607.
9 M. J. Tan, S. Zhong, J. Li, Z. Chen and W. Chen, *ACS Appl. Mater. Interfaces*, 2013, **5**, 4696–4701.
10 M. Gratzl, D. F. Hsu, A. M. Riley and J. Janata, *J. Phys. Chem.*, 1990, **94**, 5973–5981.
11 P. Marque, J. Roncali and F. Garnier, *J. Electroanal. Chem.*, 1987, **218**, 107–118.
12 S. A. M. Refaey and G. Schwitzgebel, *Des. Monomers Polym.*, 2000, **3**, 389–398.
13 B. L. Funt and S. V. Lowen, *Synth. Met.*, 1985, **11**, 129–137.
14 G. Zotti, G. Schiavon, S. Zecchin, F. Sannicolo' and E. Brenna, *Chem. Mater.*, 1995, **7**, 1464–1468.
15 Y. Li, *J. Electroanal. Chem.*, 1997, **433**, 181–186.
16 S. H. Strauss, *Chem. Rev.*, 1993, **93**, 927–942.
17 R. Cordova, M. A. d. Valle, A. Arratia, H. Gomez and R. Schrebler, *J. Electroanal. Chem.*, 1994, **377**, 75–83.
18 G. Tourillon and Y. Jugnet, *J. Chem. Phys.*, 1988, **89**, 1905–1913.
19 L. F. Warren and D. P. Anderson, *J. Electrochem. Soc.*, 1987, **134**, 101–105.
20 J. R. Reynolds, S.-G. Hsu and H. J. Arnott, *J. Polym. Sci., Part B: Polym. Phys.*, 1989, **27**, 2081–2103.
21 G. Horowitz and F. Garnier, *Sol. Energy Mater.*, 1986, **13**, 47–55.
22 A. Tsumura, H. Koezuka and T. Ando, *Synth. Met.*, 1988, **25**, 11–23.
23 F. Garnier, *Chem. Phys.*, 1998, **227**, 253–262.
24 R. J. Waltman, J. Bargon and A. F. Diaz, *J. Phys. Chem.*, 1983, **87**, 1459–1463.
25 G. Schopf and G. Koßmehl, *Polythiophenes – Electrically Conductive Polymers*, Springer-Verlag, 1997.
26 G. Morea, L. Sabbatini, P. G. Zambonin, A. J. Swift, R. H. West and J. C. Vickerman, *Macromolecules*, 1991, **24**, 3630–3637.
27 *Practical Surface Analysis*, ed. D. Briggs and M. P. Seah, John Wiley & Sons, West Sussex, 2nd edn, 1990.
28 B. J. Lindberg, K. Hamin, G. Johansson, U. Gelius, A. Fahlman, C. Nordling and K. Siegbahn, *Phys. Scr.*, 1970, **1**, 286–298.
29 C. D. Wagner, W. M. Riggs, L. E. Davis, J. F. Moulder and G. E. Muilenberg, *Handbook of X-Ray Photoelectron Spectroscopy*, Perkin-Elmer Corporation, Physical Electronics Division, Eden Prairie, 1979.
30 Y. T. Yin, W. X. Que and C. H. Kam, *J. Sol-Gel Sci. Technol.*, 2010, **53**, 605–612.
31 Y. Sun, J. H. Seo, C. J. Takacs, J. Seifter and A. J. Heeger, *Adv. Mater.*, 2011, **23**, 1679–1683.
32 E. Poverenov, M. Li, A. Bitler and M. Bendikov, *Chem. Mater.*, 2010, **22**, 4019–4025.
33 J. H. Kaufman, C. K. Baker, A. I. Nazzal, M. Flickner, O. R. Melroy and A. Kapitulnik, *Phys. Rev. Lett.*, 1986, **56**, 1932–1935.
34 S. Rangan, S. Coh, R. A. Bartynski, K. P. Chitre, E. Galoppini, C. Jaye and D. Fischer, *J. Phys. Chem. C*, 2012, **116**, 23921–23930.
35 X. T. Hao, T. Hosokai, N. Mitsuo, S. Kera, K. K. Okudaira, K. Mase and N. Ueno, *J. Phys. Chem. B*, 2007, **111**, 10365–10372.
36 K. Noori and F. Giustino, *Adv. Funct. Mater.*, 2012, **22**, 5089–5095.
37 K. Nishi, S. Arata, N. Matsumoto, S. Iijima, Y. Sunatsuki, H. Ishida and M. Kojima, *Inorg. Chem.*, 2010, **49**, 1517–1523.
38 R.-D. Schnebeck, E. Freisinger and B. Lippert, *Angew. Chem., Int. Ed.*, 1999, **38**, 168–171.
39 A. M. Bond, S. R. Ellis and A. F. Hollenkamp, *J. Am. Chem. Soc.*, 1988, **110**, 5293–5297.
40 O.-S. Jung, Y. J. Kim, Y.-A. Lee, K.-M. Park and S. S. Lee, *Inorg. Chem.*, 2003, **42**, 844–850.
41 M. G. Hill, W. M. Lamanna and K. R. Mann, *Inorg. Chem.*, 1991, **30**, 4687–4690.
42 S. Braun, W. R. Salaneck and M. Fahlman, *Adv. Mater.*, 2009, **21**, 1450–1472.
43 A. Tada, Y. Geng, Q. Wei, K. Hashimoto and K. Tajima, *Nat. Mater.*, 2011, **10**, 450–455.
44 P. Ruankham, S. Yoshikawa and T. Sagawa, *Mater. Chem. Phys.*, 2013, **141**, 278–282.
45 M. Ohyama, H. Kozuka and T. Yoko, *Thin Solid Films*, 1997, **306**, 78–85.
46 G. Gritzner and J. Kuta, *Pure Appl. Chem.*, 1984, **56**, 461–466.
47 R. R. Gagne, C. A. Koval and G. C. Lisensky, *Inorg. Chem.*, 1980, **19**, 2854–2855.
48 M. Namazian, C. Y. Lin and M. L. Coote, *J. Chem. Theory Comput.*, 2010, **6**, 2721–2725.
49 J. O'M. Bockris and S. U. M. Khan, *Surface Electrochemistry – A Molecular Level Approach*, Plenum Press, New York, 1983.
50 D. A. Arena, F. G. Curti and R. A. Bartynski, *Surf. Sci.*, 1996, **369**, L117–L121.
51 M. W. Schmidt, K. K. Baldridge, J. A. Boatz, S. T. Elbert, M. S. Gordon, J. H. Jensen, S. Koseki, N. Matsunaga, K. A. Nguyen, S. J. Su, T. L. Windus, M. Dupuis and J. A. J. Montgomery, *J. Comput. Chem.*, 1993, **14**, 1347–1363.
52 A. D. Becke, *Phys. Rev. A*, 1988, **38**, 3098–3100.
53 C. Lee, W. Yang and R. G. Parr, *Phys. Rev. B: Condens. Matter Mater. Phys.*, 1988, **37**, 785–789.
54 A. D. Becke, *J. Chem. Phys.*, 1993, **98**, 5648–5652.
55 K. L. Schuchardt, B. T. Didier, T. Elsethagen, L. Sun, V. Gurumoorthi, J. Chase, J. Li and T. L. Windus, *J. Chem. Inf. Model.*, 2007, **47**, 1045–1052.

